SCIENCE CHINA
Earth Sciences

IOD-related optimal initial errors and optimal precursors for IOD predictions from reanalysis data

FENG Rong and DUAN WanSuo

Citation: SCIENCE CHINA Earth Sciences **60**, 156 (2017); doi: 10.1007/s11430-016-0103-9

View online: http://engine.scichina.com/doi/10.1007/s11430-016-0103-9

View Table of Contents:http://engine.scichina.com/publisher/scp/journal/SCES/60/1

Published by the Science China Press

SCIENCE CHINA
Earth Sciences

• RESEARCH PAPER •

January 2017 Vol.60 No.1: 156–172
doi: 10.1007/s11430-016-0103-9

IOD-related optimal initial errors and optimal precursors for IOD predictions from reanalysis data

FENG Rong & DUAN WanSuo*

State Key Laboratory of Numerical Modeling for Atmospheric Sciences and Geophysical Fluid Dynamics (LASG), Institute of Atmospheric Physics, Chinese Academy of Sciences, Beijing 100029, China

Received September 5, 2016; accepted October 9, 2016; published online December 2, 2016

Abstract This study explored the spatial patterns of winter predictability barrier (WPB)-related optimal initial errors and optimal precursors for positive Indian Ocean dipole (IOD) events, and the associated physical mechanisms for their developments were analyzed using the Simple Ocean Data Assimilation dataset. Without consideration of the effects of model errors on "predictions," it was assumed that different "predictions" are caused by different initial conditions. The two types of WPB-related optimal initial errors are almost opposite for the start months of July (–1) and July (0), although they both present a west-east dipole pattern in the tropical Indian Ocean, with the maximum errors located at the thermocline depth. Bjerknes feedback and ocean waves play important roles in the growth of prediction errors. These two physical mechanisms compete during July–December and ocean waves dominate during January–June. The spatial patterns of optimal precursors and the physical mechanisms for their developments are similar to those of WPB-related optimal initial errors. It is worth noting that large values of WPB-related optimal initial errors and optimal precursors are concentrated within a few locations, which probably represent the sensitive areas of targeted observations for positive IOD events. The great similarities between WPB-related optimal initial errors and optimal precursors suggest that were intensive observations performed over these areas, this would not only reduce initial errors and thus, prediction errors, but it would also permit the detection of the signal of IOD events in advance, greatly improving the forecast skill of positive IOD events.

Keywords Optimal precursors, Initial errors, Winter predictability barrier, Indian Ocean dipole

Citation: Feng R, Duan W S. 2017. IOD-related optimal initial errors and optimal precursors for IOD predictions from reanalysis data. Science China Earth Sciences, 60: 156–172, doi: 10.1007/s11430-016-0103-9

1. Introduction

The Indian Ocean dipole (IOD) is a famous coupled ocean-atmosphere phenomenon of interannual time scales in the tropical Indian Ocean (Saji et al., 1999; Webster et al., 1999; Li et al., 2003). Positive IOD events have positive sea surface temperature anomalies (SSTAs) in the western Indian Ocean and negative SSTAs in the southeastern Indian Ocean, accompanied by an anomalous surface easterly wind at the equator (Saji et al., 1999; Webster et al., 1999; Li et al., 2002, 2003). Negative IOD events show the converse SSTA and surface wind patterns. The strength of IOD events is usually measured using the Dipole Mode Index (DMI), which is the difference in SSTAs between the western Indian Ocean (50°–70°E, 10°S–10°N) and southeastern Indian Ocean (90°–110°E, 10°S–Equator) (Saji et al., 1999). IOD events often reverse the sign of the DMI during the winter preceding the IOD year, then peak in September or October of the IOD year, before finally reversing the sign again in the following winter (Wajsowicz, 2004; Feng et al., 2014a). Because of the considerable climatic effects of IOD events on nearby and distant areas (Birkett et al., 1999; Black et al., 2003; Annamalai and Murtugudde, 2004), it is vital and meaningful to be able to predict IOD events accurately.

*Corresponding author (email: duanws@lasg.iap.ac.cn)

Considerable progress has been made in the study of the predictability of IOD events. Previous research has suggested that the lead time for skillfully predicting IOD events is about one season, and that it can be extended to two seasons for strong events (Wajsowicz, 2004, 2005; Luo et al., 2005, 2007; Zhao and Hendon, 2009; Shi et al., 2012). It is likely that this low forecast skill is closely related to the winter predictability barrier (WPB) phenomenon (Luo et al., 2007). From a statistical viewpoint, the WPB indicates that, regardless of start month, forecast skill drops rapidly across the boreal winter (Luo et al., 2007). From the viewpoint of error growth, the WPB means that prediction errors grow fastest in winter (Feng et al., 2014a). It should be noted that the WPB is demonstrated to exist not only in the growing phase but also in the decaying phase of IOD events. By carrying out perfect model predictability experiments, Feng et al. (2016) showed that the dominant spatial pattern of initial errors, which are most likely to cause a significant WPB in the growing and decaying phases of the IOD, presents a west-east dipole pattern in sea temperatures, both at the surface and at 95-m depth. Nevertheless, the initial errors in this study were only superimposed on two levels of the sea temperatures in the model. However, initial errors might exist within the entire ocean in practical forecasting. Therefore, further analysis is needed to explore the effects of initial errors within the entire Indian Ocean on IOD predictions.

In addition to the aforementioned initial errors that cause a significant WPB and have large effects on IOD predictions, the precursor is another important issue in the predictability of IOD events. A precursor is an initial anomaly that is likely to develop into an IOD event under the constrained conditions. The study of precursors is favorable for the identification of IOD events in advance and for then improving forecast skill. Horii et al. (2008) showed that the TRITON floats in the tropical eastern Indian Ocean had successfully detected the precursors for the three consecutive positive IOD events in 2006–2008. These were manifested as significant negative signals at the thermocline depth several months preceding the appearance of the SSTAs. This made us consider whether all positive IOD events have the same precursor with negative signals in the subsurface ocean in the tropical eastern Indian Ocean. Furthermore, Mu et al. (2016)[1)] explored the spatial patterns of the optimal initial errors and optimal precursors using a coupled model, and they demonstrated the great similarity between them. The current study considered whether this conclusion holds true using reanalysis data. Based on the above discussion, several questions are proposed: (1) What are the spatial patterns of the initial errors in the Indian Ocean that cause a significant WPB (referred to as WPB-related initial errors in the following discussion) in the growing and decaying phases of IOD events and of the initial anomalies that develop into an IOD event (i.e., the precursor)? (2) What are the respective physical mechanisms for their developments? (3) What is the relationship between the WPB-related initial errors and the precursors of positive IOD events?

Zhang et al. (2015) explored the optimal initial errors related to the spring predictability barrier and the associated physical mechanisms using pre-industrial control runs of several Coupled Model Intercomparison Project Phase 5 (CMIP5) models. They assumed the sea temperatures of 1 El Niño year in the model outputs as the "observation" and the sea temperatures of another 19 years around the El Niño year as the "predictions" to this year, where the prediction errors were caused only by the initial errors, because the external forcing related to the pre-industrial control run was time-invariant. This meant there was no effect related to model error during the predictions. Based on these assumptions, they analyzed the initial errors that caused a significant spring predictability barrier. Similarly, this approach was used by Kramer and Dijkstra (2013) to explore the sensitive areas of targeted observations for El Niño-Southern Oscillation (ENSO). The objective of this study was to answer the questions above by applying reanalysis data using a similar method. With consideration that positive IOD events generally have larger magnitudes and greater climatic impact than negative events (Ashok et al., 2001, 2003; Abram et al., 2003; Annamalai and Murtugudde, 2004; Behera et al., 2005; Cai et al., 2009), only positive IOD events were considered in this study.

2. Data and method

The Simple Ocean Data Assimilation (SODA) 2.2.4 reanalysis dataset (Carton and Giese, 2008), which covers the period 1921–2008, was used in this study to explore the WPB-related optimal initial errors and optimal precursors of positive IOD events. Its horizontal resolution is 0.5° × 0.5°, and its vertical resolution varies with depth; here, SST was taken at the depth of 5 m. The sea temperatures at different depths and wind stress were derived. As greenhouse gases are emerging as the dominant forcing during the twentieth century (Mann et al., 1998), with the linear trend of the dataset removed, the effects of external forcing could be ignored and a method similar to Zhang et al. (2015) used in the present study.

To explore the WPB-related initial errors, 10 positive IOD events (i.e., the DMI exceeds 0.5 standard deviations for three consecutive months) were chosen at random from the 88-year reanalysis dataset. The signs of the DMI of these IOD events tended to be reversed in boreal winter, reach a peak in September and October, and then decay during the

1) Mu M, Feng R, Duan W S. 2016. Relationship between optimal precursors for Indian Ocean Dipole events and optimally growing initial errors, in its prediction. J Geophys Res-Oceans, submitted

following winter, consistent with the results in Wajsowicz (2004). Then, the sea temperatures of each IOD event (i.e., the reference year) were assumed an "observation," and the sea temperatures in the 10 years preceding and the 10 years following each reference year were assumed the "predictions" to this "observation". Thus, there were 20 predictions for each "observed" IOD year and each prediction had a 12-month lead time. As mentioned above, with the linear trend of the dataset removed, the effects of external forcing could be neglected and therefore, the prediction errors here could be assumed caused only by initial errors, i.e., the different "predictions" could be assumed the results of different initial conditions.

The start months of the "predictions" were defined as July (–1) and July (0) (where "–1" signifies the year preceding the IOD year and "0" signifies the IOD year). The "predictions" starting from July (–1) (July (0)) spanned the winter of the growing (decaying) phase of the positive IOD events. The so-called growing phase signifies the period from the sign reversal of the DMI in winter to the peak of the positive IOD event. The decaying phase covers the period from the peak of the IOD event to the following sign reversal in the following winter. Specifically, for the start month July (–1), the sea temperatures from July (–1) to June (0) in each reference year were considered as the "observations," and the sea temperatures from July (–2) to June (–1) (where "–2" signifies the year preceding year "–1") were considered as 1 of the 20 "predictions," and so on (Figure 1a). Similarly, for the start month July (0), the sea temperatures from July (0) to June (1) (where "1" signifies the year following the IOD year) in each reference year were considered as the "observations," and the sea temperatures from July (1) to June (2) (where "2" signifies the year following the year "1") were considered as 1 of the 20 "predictions," and so on (Figure 1b). The prediction errors were defined as the absolute values of the difference between the "predicted" DMI and the "observed" DMI. As there were no model errors, the prediction errors were caused only by the initial errors. The initial errors of sea temperatures in the tropical Indian Ocean, which are closely related with positive IOD events, were the subject of interest in this study. They were defined as the difference in sea temperatures between the first month of the "predictions" and the first month of the corresponding "observations." To explore the WPB-related initial errors, the growth rates of prediction errors κ in each month were analyzed:

$$\kappa = \frac{\partial P(t)}{\partial t} \approx \frac{P(t_2) - P(t_1)}{t_2 - t_1}, \quad (1)$$

where $P(t_1)$ and $P(t_2)$ represent the prediction errors at time t_1 and t_2, respectively ($t_2 > t_1$; where $t_2 - t_1$ is one month and sufficiently small). A positive (negative) value of κ signifies that the prediction errors increase (decrease), and the larger the positive value of κ, the faster the prediction errors grow within one month. As the prediction errors were caused only by the initial errors, the first kind of predictability experiments were conducted to identify the role of the initial errors in IOD predictions.

Similar experiments were conducted to explore the precursors of positive IOD events. The main difference from the experiments that explored the WPB-related initial errors was that 10 normal years (i.e., not positive or negative IOD years) were chosen at random as the reference state. As IOD events usually reverse the sign of the DMI and occur in winter (Wajsowicz, 2004; Feng et al., 2014a), the start month of the predictions was defined as January. Thus, the sea temperatures of each normal year (January–December) were considered as the "reference year." The sea temperatures in the 10 years preceding and the 10 years following this reference year were assumed the "predictions" with different initial perturbations superimposed on the initial fields of this "reference year." The DMI was calculated based on the difference in sea temperatures between the "predictions" and the corresponding "reference year." If the DMI exceeded 0.5 standard deviations for three consecutive months, a positive IOD event occurred. Then, the initial perturbations, which were superimposed on the initial fields of the "normal year," developed into a positive IOD event and they could be defined as one precursor of a positive IOD. Here, the initial perturbations were calculated as the difference in sea temperatures in January between the "predictions" and the corresponding reference year.

3. Results

This section presents the results of the analysis of the season-

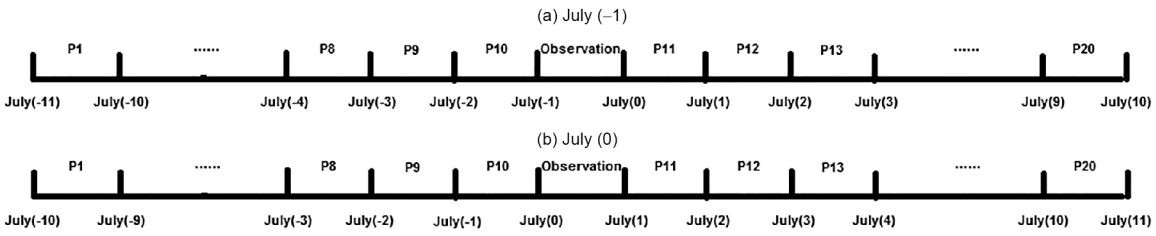

Figure 1 Schematic of the experimental design for one reference year with start months (a) July (–1) and (b) July (0). July (–11), July (–10), …, July (11) in different years along the *x*-axis indicate the first month of the predictions and observations. P1, P2, …, P20 indicate the 20 predictions for each "observation" with different initial conditions.

ally dependent evolution of prediction errors, and it identifies the dominant spatial patterns of initial errors that caused a significant WPB for positive IOD events. Then, by analyzing the evolution of these initial errors, the physical mechanism of the error growth associated with the WPB is explored. Similarly, the dominant spatial patterns of initial anomalies that develop into positive IOD events, as well as the physical mechanisms of their development, are also explored.

3.1 Spatial patterns of WPB-related optimal initial errors for positive IOD events

According to the method in section 2, we calculated the prediction errors for each "observed" positive IOD event, and the error growth rates in each month were estimated using eq. (1). As there were 20 predictions for each "observed" IOD event for start month July (–1) or July (0), the ensemble means of the monthly error growth rates for each "observed" IOD year were calculated. The ensemble means of the monthly error growth rates for the 10 reference IOD years are shown in Figure 2. It is apparent that the error growth rates are large and positive in the periods December (–1) to February (0) and April (0) to May (0) during the lifetime of positive IOD events for most reference years for start month July (–1), i.e., the prediction errors grow fastest during these two periods. According to the definition of the WPB in Feng et al. (2014a), a significant WPB occurs in the growing phase of positive IOD events. Similarly, the fast error growth in the period April (0) to May (0) corresponds to the summer predictability barrier (SPB; Luo et al., 2007), which might have a close relationship with ENSO (Luo et al., 2007). For start month July (0), the error growth rates are large and positive in the periods July (0) to August (0) and January (0) to March (0). The fast error growth in these periods corresponds to two predictability barriers: the first being the SPB and the second being the WPB in the decaying phase of positive IOD events. Based on the above discussion, it is evident that a significant WPB exists in both the growing and the decaying phases of positive IOD events, which is consistent with the results in Feng et al. (2014a). Furthermore, a significant SPB also exists during the IOD predictions. In this study, we were mainly concerned with the initial errors that cause significant WPBs in the growing and decaying phases of positive IOD events, which have great effect on predictions for the occurrence and decay of positive IOD events.

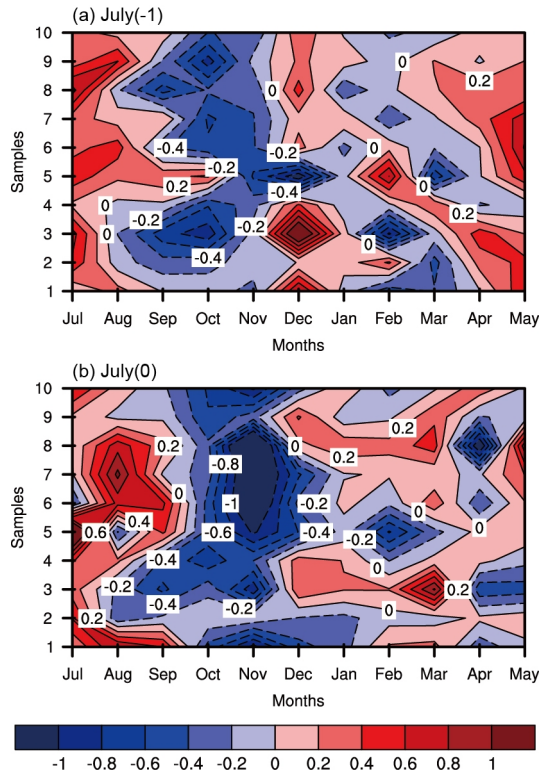

Figure 2 Ensemble mean of the monthly error growth rates for each reference IOD year (units: month^{-1}) for start months (a) July (–1), and (b) July (0). The horizontal axes denote the months from July to May. The vertical axes denote 10 reference IOD events.

By analyzing the evolutions of prediction errors, we found that some prediction errors showed significant seasonally dependent evolution with the fastest growth in boreal winter, whereas other prediction errors presented no such characteristic. According to the discussion in section 2, the prediction errors in this study were caused only by initial errors. Therefore, not all initial errors are predisposed to cause significant WPBs. The initial errors that presented seasonally dependent evolution, with the fastest error growth in winter in the growing or decaying phases, were chosen and signified as the initial errors that cause significant WPBs. In consideration that realistic initial SST errors are usually small, the selected initial errors were constrained further by the conditions that the average absolute values of the initial SST errors in the tropical Indian Ocean should be <0.5°C. After screening, there were 46 and 39 initial errors for start months July (–1) and July (0), respectively. To explore the dominant spatial patterns of these initial errors, we performed Combined Empirical Orthogonal Function (CEOF) analysis of the initial temperature errors in the tropical Indian Ocean and analyzed the leading CEOF mode (i.e., the dominant mode of the initial errors). The leading CEOF mode (i.e., CEOF1; responsible for 31.6% and 23.3% of the total variance for start month July (–1) and July (0), respectively) combined with the corresponding time series (i.e., PC1) suggested there were mainly two types of WPB-related initial errors for each start month: one type similar to the CEOF1 mode and the other type opposite to it. When the individual value of PC1 was larger than 0.5 standard deviations or smaller than –0.5 standard deviations of PC1, the corresponding initial errors were separated into two categories. The composites of these two types of initial errors were defined as type-1 and type-2 WPB-related op-

timal initial errors, respectively, because they corresponded to almost all WPB-related fast error growth in winter in each 20-year time series. Figure 3 show the spatial patterns of the WPB-related optimal initial errors for start months July (–1) and July (0).

For start month July (–1), the type-1 WPB-related optimal initial errors present negative SST errors in the western Indian Ocean and positive SST errors in the central-southeastern Indian Ocean (Figure 3a). Correspondingly, a significant west-east dipole pattern exists in the subsurface ocean (Figure 3b). For type-2 WPB-related optimal initial errors, the surface component presents positive errors in the northwestern Indian Ocean and negative errors in the southeastern Indian Ocean; and the subsurface temperature errors are almost opposite to the type-1 initial errors (Figure 3c and 3d). It is interesting to note that, for the two types of WPB-related optimal initial errors, the initial errors in the subsurface ocean are more significant than in the surface ocean, and the maximum errors are located at a depth of 80–120 m, which matches the thermocline depth exactly. In addition, the absolute values of the maximum errors in the eastern Indian Ocean are larger than in the western Indian Ocean. Furthermore, the range of positive (negative) initial errors in the eastern Indian Ocean is also larger than that of negative (positive) initial errors in the western Indian Ocean for type-1 (type-2) WPB-related optimal initial errors.

For start month July (0), the basic characteristics of the two types of WPB-related optimal initial errors are similar to those for start month July (–1), i.e., there is a significant west-east dipole pattern in the subsurface ocean and the maximum errors are located at the thermocline depth (Figure 3e–h). However, different from the results for start month July (–1),

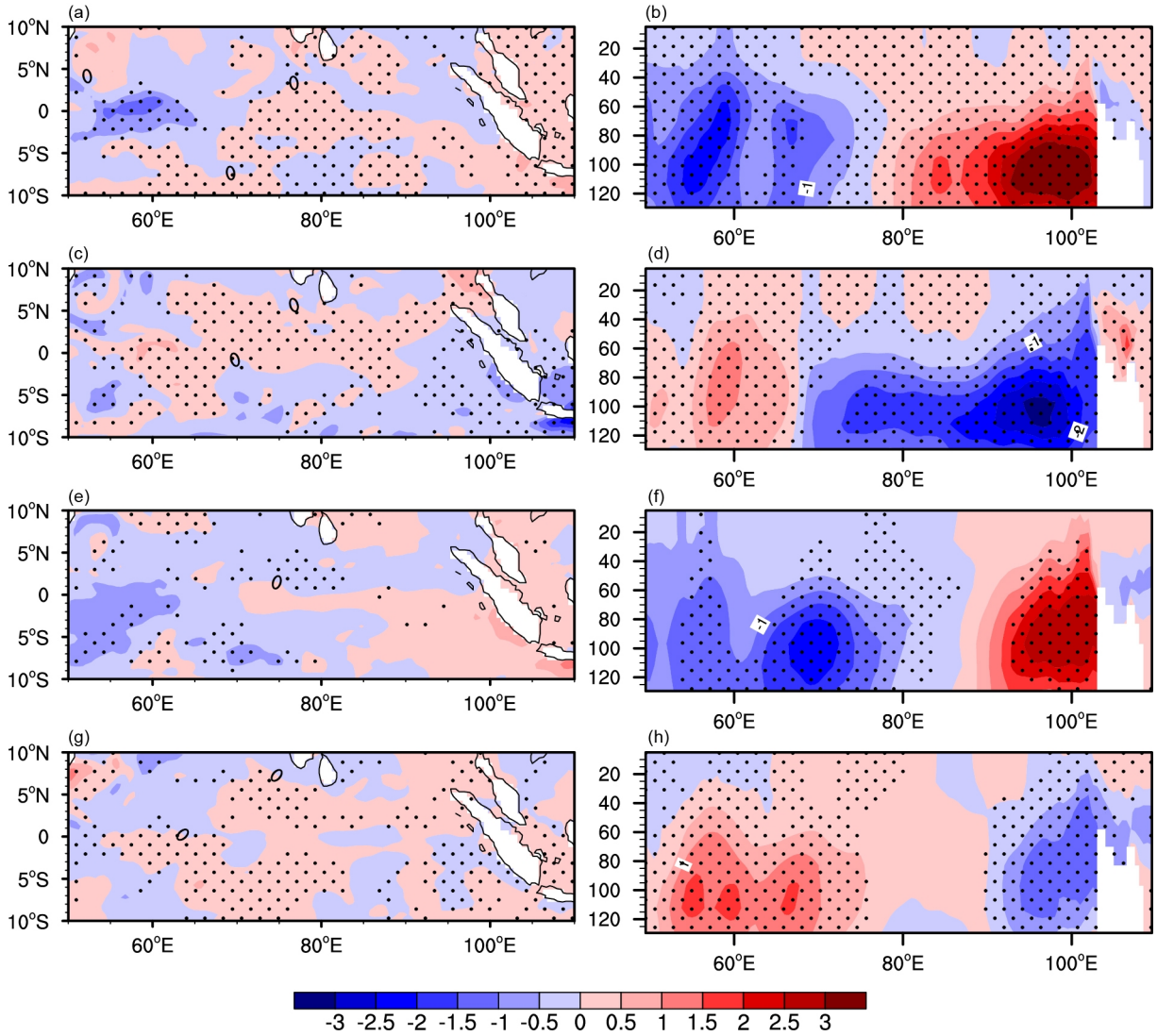

Figure 3 Spatial patterns of SST component ((a), (c), (e), (g)) and equatorial (5°S–5°N) subsurface temperature component ((b), (d), (f), (h)) of type-1 ((a), (b)) and type-2 ((c), (d)) WPB-related optimal initial errors for start month July (–1) (units: °C); ((e), (f)) and ((g), (h)) are spatial patterns of type-1 and type-2 WPB-related optimal initial errors for start month July (0), respectively. Dotted areas indicate that composites of SST and subsurface temperature errors exceed the 90% significance level, as determined by a *t*-test.

the range of errors in the eastern Indian Ocean is smaller than that of the opposite errors in the western Indian Ocean. Additionally, the absolute values of the maximum errors in the eastern Indian Ocean are smaller than in the western Indian Ocean for type-2 optimal initial errors.

The above results indicate that the initial errors with a west-east dipole pattern, especially at the thermocline depth, have great effect on IOD predictions and might constrain the forecast skill across the winter in the growing and decaying phases of positive IOD events. These findings are consistent with the results in Feng et al. (2016).

3.2 Dynamical mechanisms of error growth related to the WPB for IOD events

Having demonstrated the spatial patterns of WPB-related optimal initial errors, this section explores the effects of these initial errors on IOD predictions and analyzes the dynamical mechanisms of error growth. Figure 4 shows the evolutions of the WPB-related optimal initial errors for start month July (–1), which were calculated based on the composite difference in sea temperatures between the selected "predictions" and the corresponding "observation." When type-1 WPB-related optimal initial errors were superimposed on the initial state of positive IOD events for start month July (–1) (Figure 4a and 4b), large negative initial errors occurred in the western Indian Ocean and positive initial errors occurred in the eastern Indian Ocean, with the maximum errors located at the thermocline depth. On the one hand, the gradient of the SST errors leads to the anomalous westerly wind at the equator and therefore, the Bjerknes positive feedback works and favors the warming in eastern Indian Ocean. On the other hand, the negative subsurface temperature errors in the western equatorial Indian Ocean lift the thermocline depth. This induces an upwelling Kelvin wave that travels eastward to the eastern Indian Ocean, weakening the positive subsurface temperature errors there. Similarly, the positive subsurface temperature errors in the eastern equatorial Indian Ocean lower the thermocline depth, inducing a downwelling equatorial Rossby wave that travels westward to the western Indian Ocean, which weakens the negative subsurface temperature errors there. The subsurface temperature errors further affect the SST errors by vertical temperature advection. Based on the above, the amplification of the sea temperature errors depends on the relative importance of the two competing mechanisms. Specifically, in the first month of the predictions, the gradient of SST errors is small, which results in weak zonal anomalous winds at the equator and correspondingly, the Bjerknes positive feedback is weak. However, the subsurface temperature errors are large, indicating a considerable negative effect by ocean waves. Therefore, the role of ocean waves on sea temperature errors is greater than that of Bjerknes feedback, resulting in the weakening of the sea temperature errors in the second month. In conjunction with the decreasing of the sea temperature errors, the negative effects of the ocean waves are weakened, which is almost offset by the Bjerknes positive feedback, resulting in the sea temperature errors remaining unchanged in the following four months. In the second half of the prediction year, as the zonal wind anomalies at the equator are extremely weak, Bjerknes feedback is inactive; therefore, the ocean waves play the dominant role. The downwelling equatorial Rossby wave causes the positive subsurface temperature errors to propagate westward; and the upwelling Kelvin wave causes the negative subsurface temperature errors to propagate quickly eastward and reflect at the east coast of the Indian Ocean as the upwelling equatorial Rossby wave.

For type-2 WPB-related optimal initial errors, the primary physical mechanisms of error growth are similar to those for type-1 initial errors. In the first half of the prediction year, under the competing mechanisms, the subsurface temperature errors weaken, especially in the eastern Indian Ocean (Figure 4c and 4d). Then, in the second half of the prediction year, ocean waves play the dominant role. The upwelling equatorial Rossby wave results in the westward propagation of the negative temperature errors to the western Indian Ocean and cooling of the water there. The dowelling Kelvin wave propagates quickly eastward and reflects at the east coast of the Indian Ocean as the dowelling equatorial Rossby wave.

When the start month is July (0), the primary physical mechanisms of the error growth for the two types of WPB-related optimal initial errors are almost the same as for start month July (–1) (Figure 5). The Bjerknes positive feedback and ocean waves compete with each other in the first half of the prediction year, and the ocean waves dominate in the second half of the year. One difference, however, is that the negative temperature errors in the eastern Indian Ocean disappear quickly in the first month, and instead, positive temperature errors appear in the second month for type-2 optimal initial errors. This might have a close relation with the reversal of the equatorial wind from easterly wind anomalies to westerly wind anomalies in the first two months. Under these conditions, Bjerknes feedback, in conjunction with the role of ocean waves, favors the disappearance of the negative temperature errors and the appearance of positive errors in the eastern Indian Ocean.

The above results suggest that both Bjerknes positive feedback and ocean waves play important roles during the development of prediction errors. Generally, Bjerknes feedback is active in the first half of the prediction year (i.e., July–December) and inactive in the later period (i.e., January–June), which might have a close relation with wind strength. Thus, the two physical mechanisms compete with each other in the first half of the prediction year, resulting in the temperature errors remaining unchanged or weakening, whereas ocean waves dominate in the second half of the prediction year.

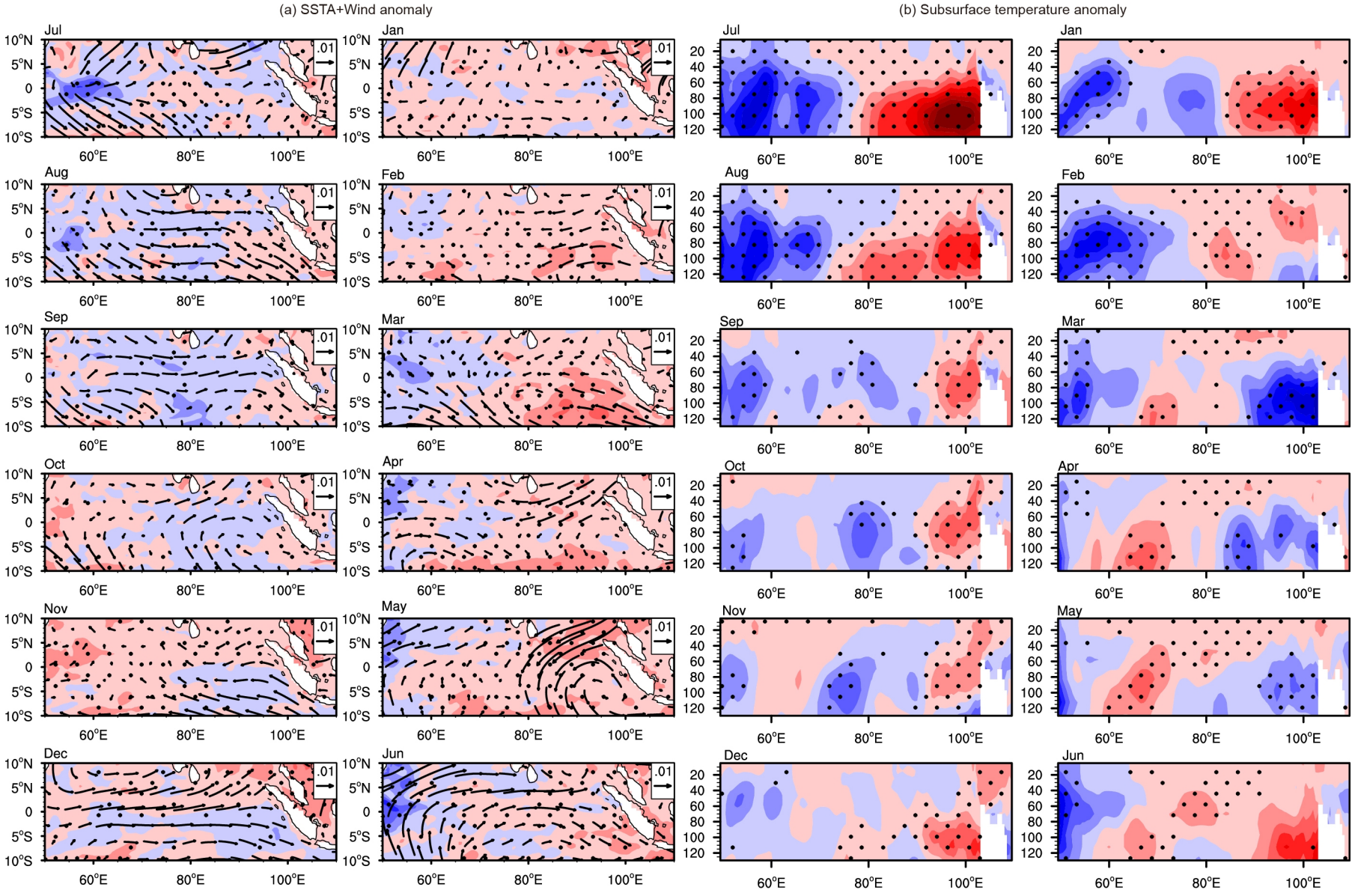

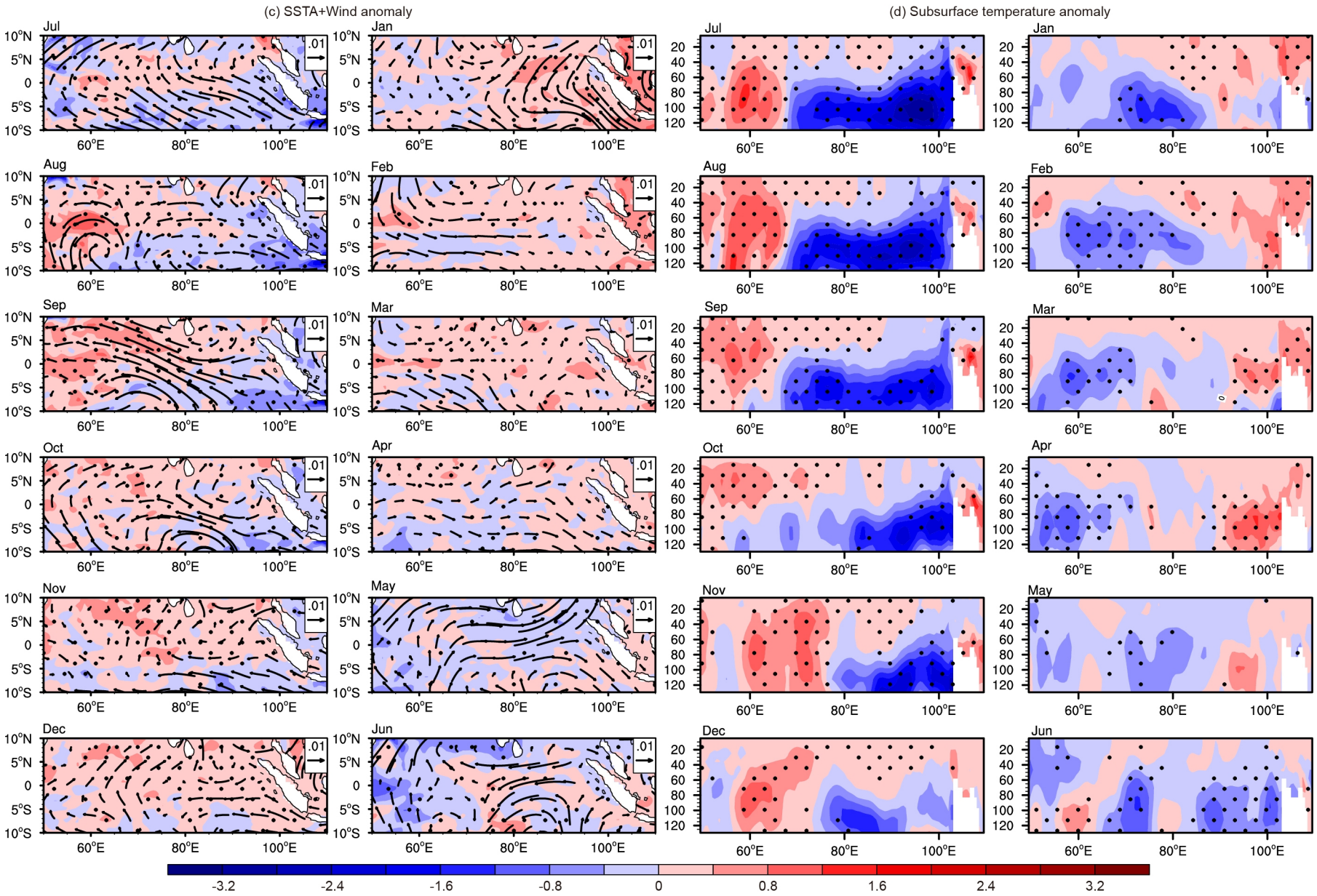

Figure 4 Evolutions of SSTA (units: °C) and sea surface wind anomaly (units: m s^{-1}) over the tropical Indian Ocean (left column) and equatorial (5°S–5°N) subsurface temperature anomaly (units: °C; right column) for type-1 ((a), (b)) and type-2 ((c), (d)) WPB-related optimal initial errors for start month July (–1). Dotted areas indicate that the composites of SST and subsurface temperature errors exceed the 90% significance level, as determined by a *t*-test.

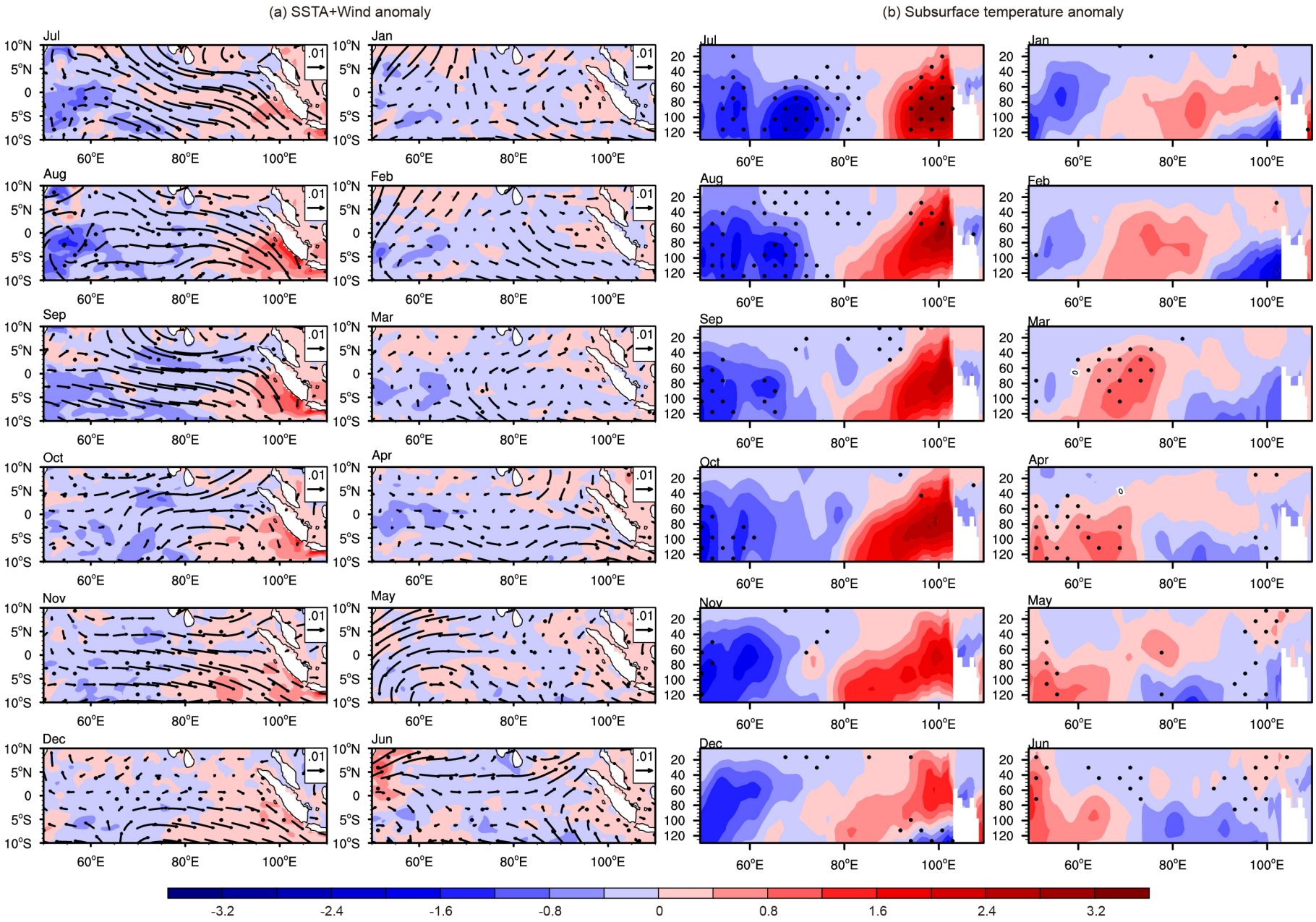

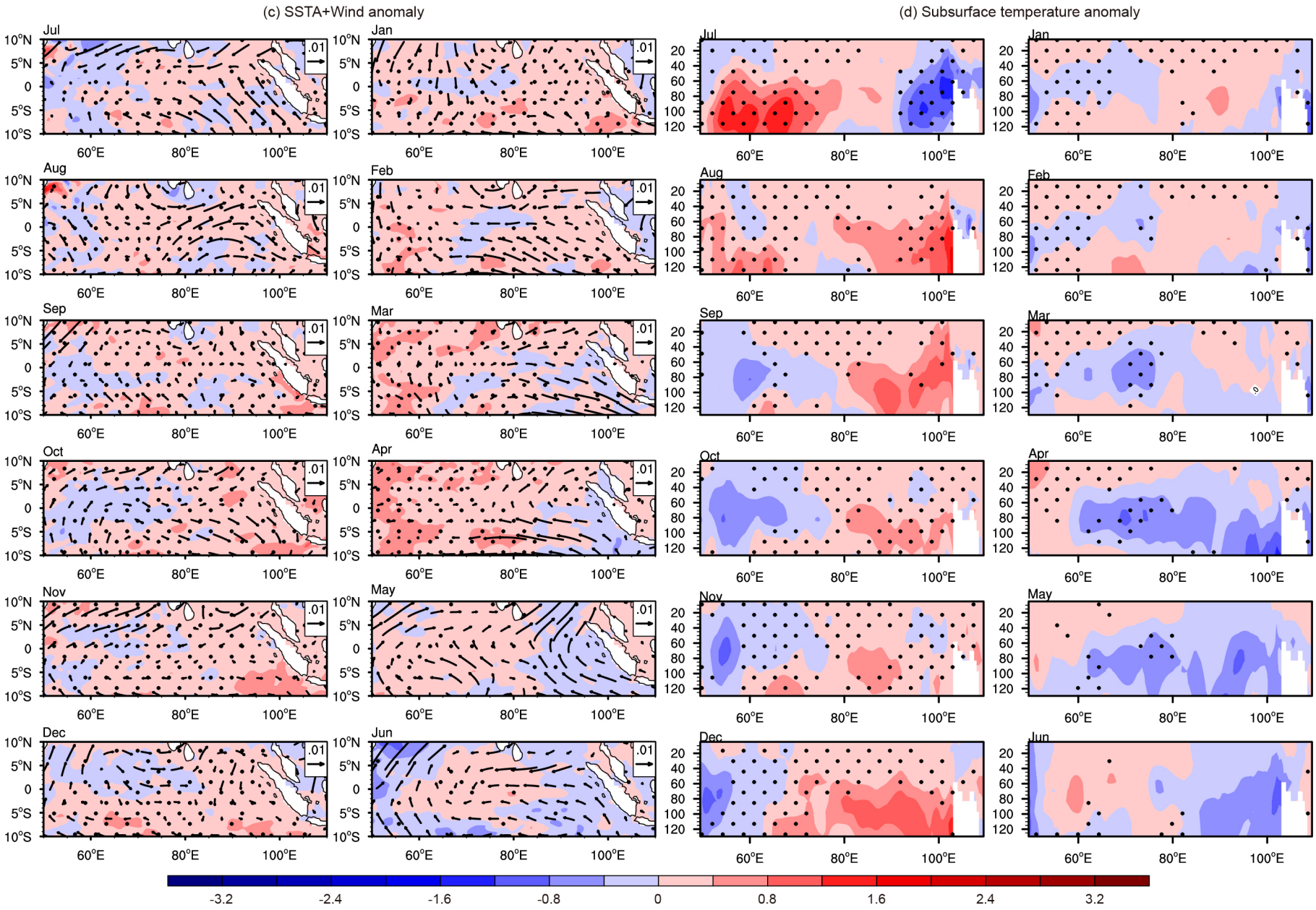

Figure 5 Evolutions of SSTA (units: °C) and sea surface wind anomaly (units: m s^{-1}) over the tropical Indian Ocean (left column) and equatorial (5°S–5°N) subsurface temperature anomaly (units: °C; right column) for type-1 ((a), (b)) and type-2 ((c), (d)) WPB-related optimal initial errors for start month July (0). Dotted areas indicate that the composites of SST and subsurface temperature errors exceed the 90% significance level, as determined by a *t*-test.

3.3 Spatial patterns of optimal precursors that develop into positive IOD events

In the previous sections, we discussed the WPB-related optimal initial errors and defined 10 positive IOD events as reference states. In this section, we replace the reference states with 10 normal years and explore the initial anomalies that develop into positive IOD events, which is also an important issue in the predictability of IOD events.

To explore the precursors of positive IOD events, initial anomalies that developed into positive IOD events were chosen according to the method in section 2. Then, we applied the CEOF analysis to these initial anomalies in the tropical Indian Ocean and analyzed the leading CEOF mode (i.e., CEOF1; responsible for 33.6% of the total variance), which describes the dominant mode of these selected initial anomalies. Similar to the WPB-related initial errors, these initial anomalies could also be divided into two categories according to the sign of the PC1 with one type similar to the CEOF1 mode and the other type opposite to it. In particular, when the individual value of the PC1 was larger than 0.5 or smaller than –0.5 standard deviations of PC1, the corresponding initial anomalies were selected. Because they corresponded to almost all positive IOD events in the 20-year SST time series, the composites of these two types of initial anomalies could be considered as the optimal precursors for positive IOD events, which were defined as type-1 and type-2 optimal precursors (Figure 6).

For a type-1 optimal precursor, SSTAs are negative in most parts of the tropical Indian Ocean, with a small area of positive SSTAs in the southeastern Indian Ocean. In the subsurface ocean, there is a significant dipole pattern with negative anomalies in the western Indian Ocean and positive anomalies in the central-eastern Indian Ocean, and the maximum anomalies are located at the thermocline depth. The type-2 optimal precursor is almost the opposite of the type-1 optimal precursor. The negative initial anomalies at the thermocline depth in the eastern Indian Ocean for type-2 optimal precursor are consistent with the results in Horii et al. (2008). Interestingly, the spatial pattern of type-1 (type-2) optimal precursor in the subsurface ocean is similar to that of the type-1 (type-2) WPB-related optimal initial errors for start months July (–1) and July (0), with a significant west-east dipole pattern. However, the SSTAs for the two types of optimal precursors mainly present a basin-wide warming or cooling, which is different from the WPB-related optimal initial errors.

The above discussion indicates that the optimal precursors of positive IOD events present a west-east dipole pattern in the subsurface ocean, with maximum anomalies located at the thermocline depth, which is similar to the WPB-related optimal initial errors. Therefore, the question addressed in the following section is whether the physical mechanisms of the development for optimal precursors are similar to those for the WPB-related optimal initial errors.

3.4 Dynamical mechanisms for the developments of optimal precursors

Similar to the discussion in section 3.2, we analyzed the developments of sea temperature anomalies for two types of optimal precursors, as well as the closely related wind stress, to explore the associated dynamical mechanisms. Figure 7 shows the evolutions of the optimal precursors, which are calculated based on the composite difference in sea temperatures between the selected "predictions" and the corresponding "normal year."

For the type-1 optimal precursor, the initial anomalies are superimposed on the initial state of the normal year (i.e., the

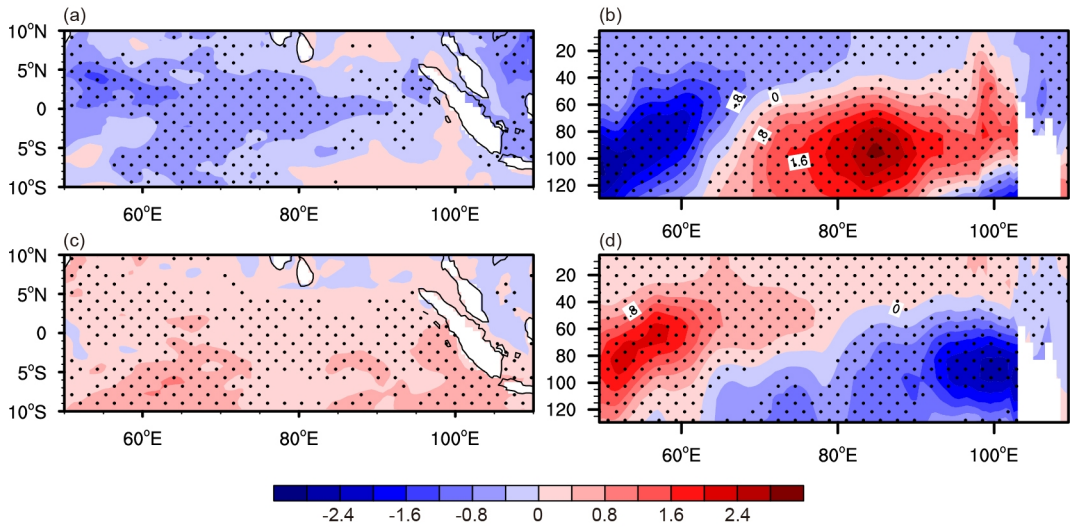

Figure 6 Spatial patterns of SST component ((a), (c)) and equatorial (5°S–5°N) subsurface temperature component ((b), (d)) of type-1 ((a), (b)) and type-2 ((c), (d)) optimal precursors (units: °C). Dotted areas indicate that composites of SSTA and subsurface temperature anomalies exceed the 90% significance level, as determined by a *t*-test.

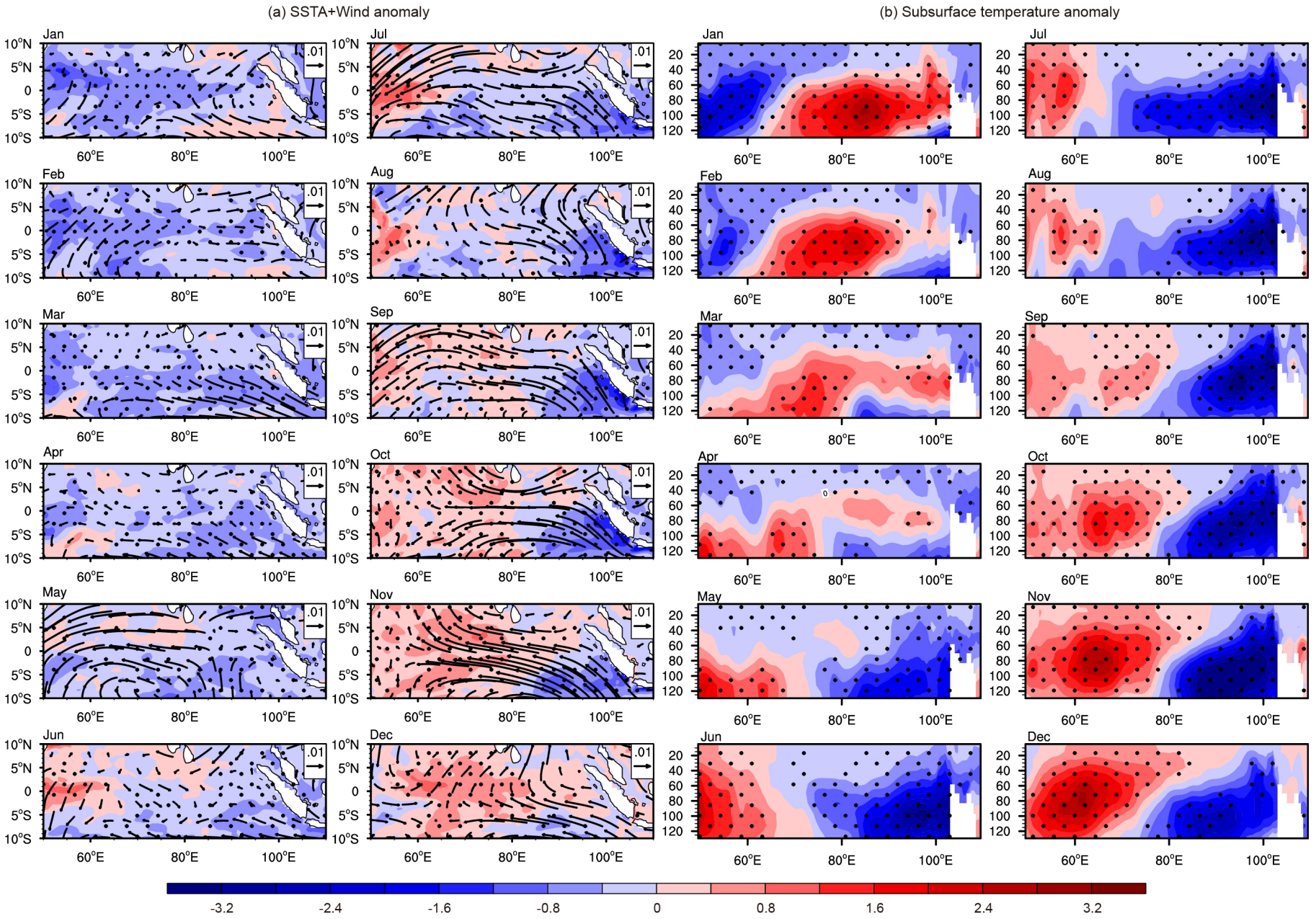

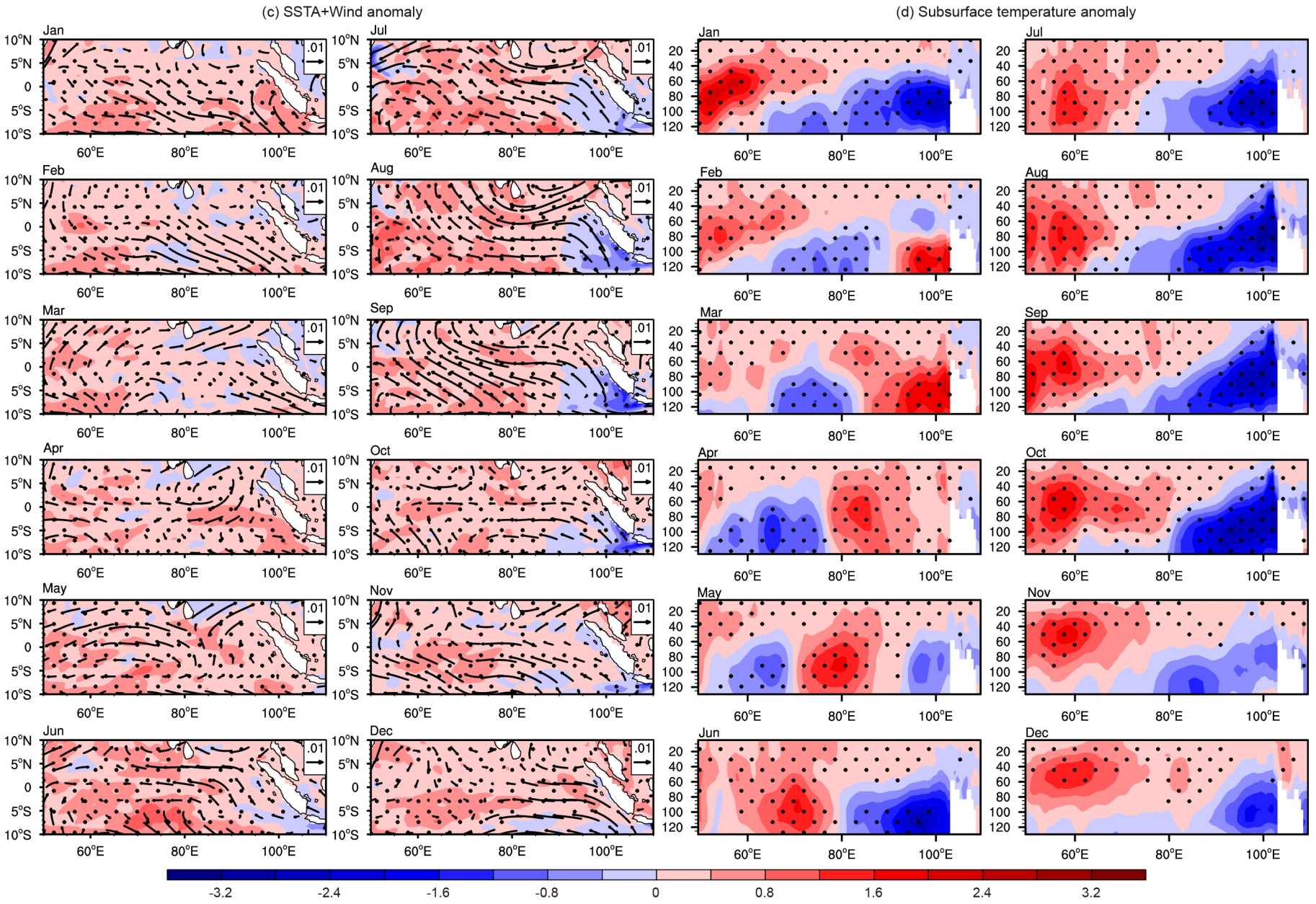

Figure 7 Evolutions of SSTA (units: °C) and sea surface wind anomaly (units: m s^{-1}) over the tropical Indian Ocean (left column), and equatorial (5°S–5°N) subsurface temperature anomaly (units: °C; right column) for type-1 ((a), (b)) and type-2 ((c), (d)) optimal precursors. Dotted areas indicate that the composites of SSTA and subsurface temperature anomalies exceed the 90% significance level, as determined by a *t*-test.

reference year), with negative anomalies in the western Indian Ocean and positive anomalies in the eastern Indian Ocean (Figure 7a and 7b) in the subsurface ocean. According to section 3.2, the amplification or reduction of sea temperature anomalies mainly depends on the relative importance between ocean waves and Bjerknes positive feedback. In the first four months, the SSTAs are basin-wide cooling, resulting in extremely weak zonal wind anomalies at the equator. Hence, Bjerknes feedback is inactive and ocean waves dominate the propagation of sea temperature anomalies. The downwelling equatorial Rossby wave causes the positive subsurface temperature anomalies to propagate westward to the western Indian Ocean, weakening the negative anomalies there. The upwelling Kelvin wave causes negative subsurface temperature anomalies to propagate quickly eastward to the east coast of the Indian Ocean. In May, the zonal wind anomalies at the equator are amplified, activating Bjerknes positive feedback. Meanwhile, the subsurface temperature anomalies are small, leading to weak effects by the ocean waves. The combination of the strong Bjerknes positive feedback and weak effects of ocean waves amplifies the temperature anomalies in the eastern Indian Ocean. From May onward, together with the intensification of the zonal wind anomalies at the equator, the Bjerknes feedback is strengthened and it dominates the growth of the sea temperature anomalies, resulting in a significant positive IOD event.

Similarly, for the type-2 optimal precursor, the Bjerknes positive feedback and ocean waves compete with each other and play important roles in the development of the initial anomalies (Figure 7c and 7d). However, ocean waves dominate for a longer time than for the type-1 optimal precursor, with negative anomalies propagating westward, which are followed by positive anomalies in the first half of the prediction year. Thus, the upwelling equatorial Rossby wave causes the negative subsurface temperature anomalies to propagate westward to the western Indian Ocean, whereas the downwelling Kelvin wave causes the positive subsurface temperature anomalies to propagate quickly eastward to the east coast of the Indian Ocean and reflect as the downwelling equatorial Rossby wave. Then, the positive subsurface temperature anomalies propagate westward under the effects of the downwelling equatorial Rossby wave. The Bjerknes feedback dominates in the second half of the prediction year, finally leading to a positive IOD event. Interestingly, although the two types of optimal precursors have opposite patterns, they both develop into positive IOD events, which might have a close relation with the different lengths of time that the two competing mechanisms dominate.

To explore the different effects of type-1 and type-2 optimal precursors on positive IOD events further, the DMIs of each were analyzed (Figure 8). For a type-1 optimal precursor, the DMI usually reverses its sign in the period February–May, peaks in October and November, and finally decays in December. However, the DMI shows a later sign reversal and earlier peak for type-2 optimal precursors. Furthermore, the amplitudes of the positive IOD events induced by type-1 optimal precursors are significantly larger than induced by type-2 optimal precursors. Therefore, except for the precursor discussed in Horii et al. (2008), another type of optimal precursor also exists for positive IOD events, which is predisposed to cause stronger positive IOD events.

The discussion in this section suggests that both ocean waves and Bjerknes feedback play important roles in the development of positive IOD events, and that Bjerknes feedback is generally inactive during the period January–June and active in the rest of the year. These results are consistent with those for WPB-related optimal initial errors. It is interesting to find that significant similarities exist between the WPB-related optimal initial errors and optimal precursors both in their spatial patterns and in the associated physical mechanisms, which are analyzed further in section 4.

4. Similarities between the WPB-related optimal initial errors and optimal precursors for positive IOD events

The similarities between the WPB-related optimal initial errors and optimal precursors for positive IOD events are discussed in terms of the following three aspects. First, both the WPB-related optimal initial errors and optimal precursors present a west-east dipole pattern in the subsurface ocean, with the maximum perturbations (i.e., maximum initial errors or maximum initial anomalies) located at the thermocline depth. This is consistent with the conclusion in Mu et al. (2016)[1]. The similarity coefficients between them are shown

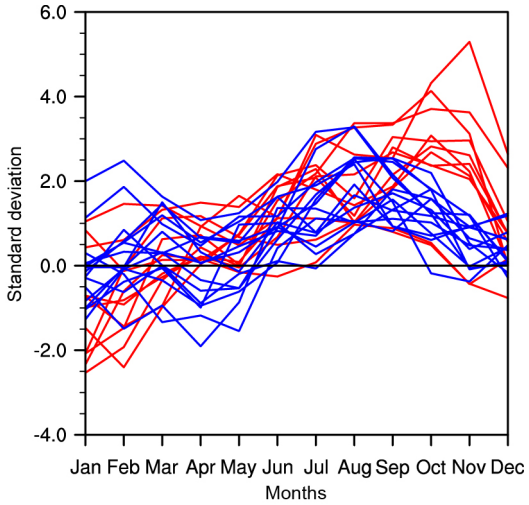

Figure 8 Time-dependent DMIs for each individual. The red lines represent the DMI for type-1 optimal precursors and the blue lines represent the DMI for type-2 optimal precursors.

in Table 1. Apparently, the optimal precursors have considerable spatial similarity with the WPB-related optimal initial errors for positive IOD events, especially with optimal initial errors for start month July (–1). Second, ocean waves and Bjerknes positive feedback play important roles in the developments of WPB-related optimal initial errors and optimal precursors. In particular, these two physical mechanisms compete with each other in the period July–December when Bjerknes feedback is active, although ocean waves dominate in the remainder of the year when Bjerknes feedback is inactive.

In addition, the WPB-related optimal initial errors and optimal precursors show similar seasonally dependent growth. The WPB-related optimal initial errors grow fastest in winter and cause a significant WPB. Feng et al. (2014b) suggested that positive IOD events show fast growth in winter in close association with the winter persistence barrier. It would be easy to deduce that the optimal precursors that develop into positive IOD events usually present fast growth in winter. The fast growth of the perturbations (i.e., WPB-related optimal initial errors and optimal precursors) has a close relationship with the weakest coupled system in winter (Feng et al., 2014b), which is favorable for the rapid variation of perturbations, resulting in the WPB and winter persistence barrier.

The discussion in section 3 suggests that the large values of the WPB-related optimal initial errors are mainly located at the thermocline depth, especially in the eastern Indian Ocean. Thus, these large values are concentrated within a few locations, and the errors over these areas have considerable effect on IOD predictions. Therefore, these areas probably represent the potential sensitive areas of targeted observations for positive IOD events. If intensive observations were conducted over these areas, the initial errors would be largely reduced, which would reduce the prediction errors and improve the forecast skill of positive IOD events considerably. Furthermore, because of the similarity of the optimal precursors to the WPB-related optimal initial errors, performing intensive observations would also detect the signals of the optimal precursors that trigger IOD events.

5. Discussion and conclusions

In this study, we explored the spatial patterns of WPB-related optimal initial errors and optimal precursors of positive IOD events and analyzed the associated physical mechanisms for their developments using the SODA dataset. As there were no model errors, the different "predictions" were caused only by different initial conditions. It was found that a significant WPB exists in both the growing and decaying phases of positive IOD events. Furthermore, a significant SPB exists during IOD predictions, which is closely related with ENSO. These results are consistent with those of Feng et al. (2014a) and Luo et al. (2007).

Initial errors that presented seasonally dependent evolutions with the fastest error growth in winter were chosen and analyzed. For start month July (–1), the type-1 WPB-related optimal initial errors presented a west-east dipole pattern in the tropical Indian Ocean, with the maximum errors located at the thermocline depth. The type-2 WPB-related optimal initial errors showed an opposite pattern to type-1. For start month July (0), the basic characteristics of the two types of WPB-related optimal initial errors were similar to those for start month July (–1). These results indicate that the initial errors with a west-east dipole pattern, especially at the thermocline depth, have considerable effect on IOD predictions and might constrain the forecast skill across the winter in the growing and decaying phases of positive IOD events; findings are consistent with the results of Feng et al. (2016).

By analyzing the developments of WPB-related optimal initial errors, it was found that Bjerknes positive feedback and ocean waves play important roles in the development of prediction errors for start months July (–1) and July (0). The two physical mechanisms compete with each other in the first half of the prediction year (i.e., July–December), resulting in the temperature errors remaining unchanged or weakening, whereas ocean waves dominate in the second half of the prediction year (i.e., January–June). Mu et al. (2016)[1)] explored the evolution of optimal initial errors using the Geophysical Fluid Dynamics Laboratory Climate Model version 2p1 (GFDL CM2p1), and the results of the current study using reanalysis data further verify their conclusions. Furthermore, the weakest coupled system in winter (Feng et al., 2014b) favors the rapid variation of perturbations under the two competing physical mechanisms, resulting in the occurrence of a significant WPB.

The optimal precursors of positive IOD events were also explored. The type-1 optimal precursor presented a significant west-east dipole pattern in the subsurface ocean. The type-2 optimal precursor was almost the opposite of type-1, and the negative initial anomalies in the eastern Indian Ocean at the thermocline depth were found consistent with the re-

Table 1 Spatial similarity coefficients between the WPB-related optimal initial errors (OE) for start months July (–1) and July (0) and optimal precursors (OP)

Similarity coefficients	OE July (–1)		OE July (0)	
	Type-1	Type-2	Type-1	Type-2
OP Type-1	0.5773	−0.6599	0.2741	−0.3001
OP Type-2	−0.8031	0.7298	−0.5909	0.5032

sults in Horii et al. (2008). Interestingly, the spatial patterns of the two types of optimal precursors were similar to those of the two types of WPB-related optimal initial errors. The physical mechanisms for the developments of the optimal precursors were analyzed further. It was found that ocean waves dominate in the first half of the prediction year, whereas Bjerknes feedback competes with ocean waves and dominates in the second half of the prediction year, finally leading to a positive IOD event. These results are consistent with the conclusions in Mu et al. (2016)[1)] based on a coupled model. In addition, although the two types of optimal precursors displayed opposite patterns, they both developed into positive IOD events, with the type-1 optimal precursor causing the stronger event.

Based on the above discussion, the WPB-related optimal initial errors and optimal precursors were found to have considerable similarities in the following three aspects. First, they both presented a west-east dipole pattern in the subsurface ocean, with the maximum perturbations located at the thermocline depth. Second, ocean waves and Bjerknes positive feedback play important roles in their developments. Furthermore, they both presented a fast growth in winter, corresponding to the WPB and winter persistence barrier, respectively. This fast growth in winter has a close relationship with the weakest coupled system in winter (Feng et al., 2014b), which is favorable for the rapid variation of perturbations. It is worth noting that the WPB-related optimal initial errors and optimal precursors showed great similarity in their spatial patterns and the largest values of these patterns were concentrated within a few locations, which probably represent the potential sensitive areas of targeted observations for positive IOD events. Therefore, should intensive observations be performed over these areas, it would not only decrease the initial errors and reduce the prediction errors further, but it would also detect the signals of the optimal precursors that trigger IOD events, greatly improving the forecast skill of positive IOD events. Similar results have been obtained in studies of ENSO and the Kuroshio large meander (Wang et al., 2013; Mu et al., 2014; Hu and Duan, 2016), and the large values of the optimal initial errors and optimal precursors, which are located within small areas, have been demonstrated to be the sensitive areas of targeted observations for these events.

To examine the spatial patterns of WPB-related optimal initial errors and optimal precursors for positive IOD events, only the initial errors and initial anomalies in sea temperature in the tropical Indian Ocean were analyzed. In fact, initial errors and initial anomalies also exist in other atmospheric and oceanic variables in the global oceans. In consideration of the interactions among different basins of the Pacific, Atlantic, and Indian oceans, it would be worthwhile to investigate the effects of these oceans on IOD predictions. Furthermore, it would be informative to explore the effects of other oceanic and atmospheric variables on IOD predictions. This study identified potential sensitive areas; however, additional sensitivity experiments should be conducted using coupled numerical models to examine the validity of these areas with regard to improving the forecast skill of positive IOD events.

Acknowledgements *This work was sponsored jointly by the National Programme on Global Change and Air-Sea Interaction (Grant No. GASI-IPOVAI-06) and the National Natural Science Foundation of China (Grant Nos. 41506032 & 41530961).*

References

Abram N J, Gagan M K, McCulloch M T, Chappell J, Hantoro W S. 2003. Coral reef death during the 1997 Indian Ocean dipole linked to Indonesian wildfires. Science, 301: 952–955

Annamalai H, Murtugudde R. 2004. Role of the Indian Ocean in regional climate variability. In: Wang C, Xie S P, Carton J A, eds. Earth Climate: The Ocean-Atmosphere Interaction. Amer Geophys Union, 147: 213–246

Ashok K, Guan Z, Yamagata T. 2001. Impact of the Indian Ocean dipole on the relationship between the Indian monsoon rainfall and ENSO. Geophys Res Lett, 28: 4499–4502

Ashok K, Guan Z, Yamagata T. 2003. Influence of the Indian Ocean dipole on the Australian winter rainfall. Geophys Res Lett, 30: 1821

Behera S K, Luo J J, Masson S, Delecluse P, Gualdi S, Navarra A, Yamagata T. 2005. Paramount impact of the Indian Ocean dipole on the East African short rains: A CGCM study. J Clim, 18: 4514–4530

Birkett C, Murtugudde R, Allan T. 1999. Indian Ocean climate event brings floods to East Africa's lakes and the Sudd Marsh. Geophys Res Lett, 26: 1031–1034

Black E, Slingo J, Sperber K R. 2003. An observational study of the relationship between excessively strong short rains in Coastal East Africa and Indian Ocean SST. Mon Weather Rev, 131: 74–94

Cai W, Cowan T, Sullivan A. 2009. Recent unprecedented skewness towards positive Indian Ocean dipole occurrences and its impact on Australian rainfall. Geophys Res Lett, 36: L11705

Carton J A, Giese B S. 2008. A reanalysis of ocean climate using simple ocean data assimilation (SODA). Mon Weather Rev, 136: 2999–3017

Feng R, Duan W S, Mu M. 2014a. The "winter predictability barrier" for IOD events and its error growth dynamics: Results from a fully coupled GCM. J Geophys Res: Oceans, 119: 8688–8708

Feng R, Mu M, Duan W. 2014b. Study on the "winter persistence barrier" of Indian Ocean dipole events using observation data and CMIP5 model outputs. Theor Appl Climatol, 118: 523–534

Feng R, Duan W, Mu M. 2016. Estimating observing locations for advancing beyond the winter predictability barrier of Indian Ocean dipole event predictions. Clim Dyn, doi: 10.1007/s00382-016-3134-3

Horii T, Hase H, Ueki I, Masumoto Y. 2008. Oceanic precondition and evolution of the 2006 Indian Ocean dipole. Geophys Res Lett, 35: L03607

Hu J, Duan W. 2016. Relationship between optimal precursory disturbances and optimally growing initial errors associated with ENSO events: Implications to target observations for ENSO prediction. J Geophys Res Oceans, 121: 2901–2917

Kramer W, Dijkstra H A. 2013. Optimal localized observations for advancing beyond the ENSO predictability barrier. Nonlin Processes Geophys, 20: 221–230

Li T, Zhang Y, Lu E, Wang D. 2002. Relative role of dynamic and thermodynamic processes in the development of the Indian Ocean dipole: An OGCM diagnosis. Geophys Res Lett, 29: 25-1–25-4

Li T, Wang B, Chang C P, Zhang Y. 2003. A theory for the Indian Ocean dipole—Zonal mode. J Atmos Sci, 60: 2119–2135

Luo J J, Masson S, Behera S, Shingu S, Yamagata T. 2005. Seasonal climate

predictability in a coupled OAGCM Using a different approach for ensemble forecasts. J Clim, 18: 4474–4497
Luo J J, Masson S, Behera S, Yamagata T. 2007. Experimental forecasts of the Indian Ocean dipole using a coupled OAGCM. J Clim, 20: 2178–2190
Mann M E, Bradley R S, Hughes M K. 1998. Global-scale temperature patterns and climate forcing over the past six centuries. Nature, 392: 779–787
Mu M, Yu Y, Xu H, Gong T. 2014. Similarities between optimal precursors for ENSO events and optimally growing initial errors in El Niño predictions. Theor Appl Climatol, 115: 461–469
Saji N H, Goswami B N, Vinayachandran P N, Yamagata T. 1999. A dipole mode in the tropical Indian Ocean. Nature, 401: 360–363
Shi L, Hendon H H, Alves O, Luo J J, Balmaseda M, Anderson D. 2012. How Predictable is the Indian Ocean dipole? Mon Weather Rev, 140: 3867–3884
Wajsowicz R C. 2004. Climate variability over the tropical Indian Ocean sector in the NSIPP seasonal forecast system. J Clim, 17: 4783–4804
Wajsowicz R C. 2005. Potential predictability of tropical Indian Ocean SST anomalies. Geophys Res Lett, 32: L24702
Wang Q, Mu M, Dijkstra H A. 2013. The similarity between optimal precursor and optimally growing initial error in prediction of Kuroshio large meander and its application to targeted observation. J Geophys Res Oceans, 118: 869–884
Webster P J, Moore A M, Loschnigg J P, Leben R R. 1999. Coupled ocean-atmosphere dynamics in the Indian Ocean during 1997–98. Nature, 401: 356–360
Zhang J, Duan W S, Zhi X F. 2015. Using CMIP5 model outputs to investigate the initial errors that cause the “spring predictability barrier” for El Niño events. Sci China Earth Sci, 58: 685–696
Zhao M, Hendon H H. 2009. Representation and prediction of the Indian Ocean dipole in the POAMA seasonal forecast model. Q J R Meteorol Soc, 135: 337–352